Accident Detection System for Bicycle Riders

Fatemehsadat Tabei, *Graduate Student Member, IEEE*,
Behnam Askarian, *Graduate Student Member, IEEE*,
and Jo Woon Chong, *Member, IEEE*

***Abstract*—Bicycle riders are exposed to accident injuries such as head trauma. The risk of these riders' injuries is higher compared to the risk of injuries for motorists. Crashes, riders' errors, and environmental hazards are the cause of bicycle-related accidents. In 2017, nearly 50% of bicycle-related accidents occurred in urban areas at night, which may contribute to a delay in reporting the accidents to emergency centers. Hence, a system that can detect the accident is needed to notify urgent care clinics promptly. In this article, we propose a bicycle accident detection system. We designed hardware modules measuring the features related to the riding status of a bicycle and fall accidents. For this purpose, we used a magnetic, angular rate, and gravity (MARG) sensor-based system which measures four different types of signals: 1) acceleration, 2) angular velocity, 3) angle, and 4) magnitude of the riding status. Each of these signals is measured in three different directions (*X*, *Y*, and *Z*). We used two different time-domain parameters, i.e., average and standard deviation. As a result, we considered 24 features. We used principal component analysis (PCA) for feature reduction and the support vector machines (SVM) algorithm for the detection of fall accidents. Experimental results show that our proposed system detects fall accidents during cycling status with 95.2% accuracy, which demonstrates the feasibility of our proposed bicycle accident detection system.**

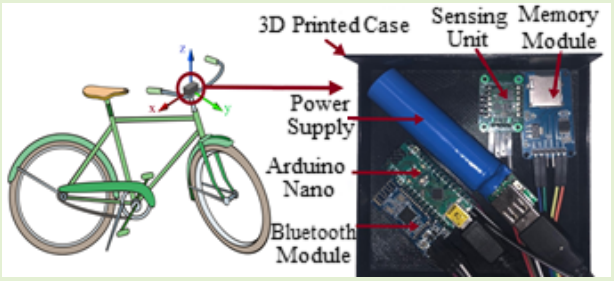

***Index Terms*—Bicycle accident, fall detection, MARG, principal component analysis, support vector machines.**

I. Introduction

ACCORDING to the Centers for Disease Control and Prevention's (CDC) report published in 2017 [1], bicycle-related accidents lead to around 1,000 fatal and 467,000 non-fatal injuries. There are various causes associated with these bicycle-related accidents such as rider's carelessness, environmental hazards, and crashes with motor vehicles or other bicycles [2]. More than 45% of bicycle-related accidents are reported to occur in dark conditions and urban areas [1], [3]. Moreover, in some situations, the rider may be alone or unable to ask for help due to shock, injuries, or unconsciousness, which can delay medical treatment [4].

There have been studies on analyzing and monitoring riding conditions to increase the safety of bicycle riders [3], [5]–[10]. In [9], a smartphone is used to recognize four different types of riding status - right turn, left turn, straight run, and stop. Here, the smartphone was attached to a bicycle handlebar and collected accelerometer and gyroscope data to recognize the movement type of the bicycle based on data [9]. In [10], Global Positioning System (GPS) data, as well as accelerometer and gyroscope data of a smartphone, were used to send an alarm signal to the bicycle rider when the bicycle is heading toward a wrong direction. Collisions with bicycle riders or pedestrians during car driving were simulated in [3]. A collision avoidance method for bicycle riders, which detected approaching vehicles using a smartphone, was proposed in [6]. A vehicle to vehicle (V2V) network-based bicycle rider detection method for car drivers, which provided driver assistance, was proposed in [7]. A bicycle rider detection algorithm for car drivers was also proposed in [8] where bicycles were detected using images captured by a stereo camera mounted on a vehicle. However, pre-accident or accident detection methods for bicycle riders, which detect accidents caused by environmental hazards such as road hazards (potholes, sewer grates, and any object in the road), or failure of the bicycle's mechanical system, have not been considered in these studies.

There have also been studies on monitoring the safety of motorcyclists [11]–[13]. In [11], data gathered from four triaxial accelerometer sensors placed on a motorcycle were used for hazard detection. A black box system having an accelerometer and GPS unit was designed to monitor and detect accidents as well as to store a motorcyclist's accident history [12]. In [13], accelerometer signals were used for motorcyclists to detect fall accidents based on threshold values. In addition to these studies, research on detecting a person's fall has been widely

Manuscript received July 3, 2020; revised August 20, 2020; accepted August 20, 2020. Date of publication September 3, 2020; date of current version December 16, 2020. The associate editor coordinating the review of this article and approving it for publication was Prof. Octavian Postolache. *(Corresponding author: Jo Woon Chong.)*

The authors are with the Department of Electrical and Computer Engineering, Texas Tech University, Lubbock, TX 79409 USA (e-mail: j.chong@ttu.edu).

Digital Object Identifier 10.1109/JSEN.2020.3021652

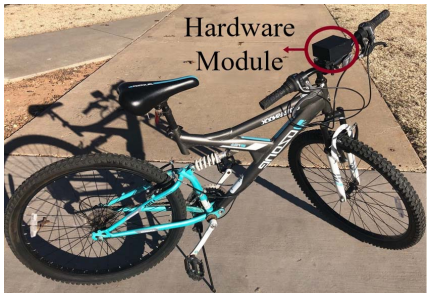

Fig. 1. The proposed hardware module for bicycle accident detection. The module is attached to the bicycle handlebar.

conducted [14]–[29]. Especially in [27]–[29], a smartphone was used to detect and locate fall accidents.

In this article, we propose a magnetic, angular rate, and gravity (MARG) sensor-based accident detection system for bicycle riders. The system detects accident-related movements of a bicycle, i.e., collisions with motor vehicles (e.g., cars, buses, motorcycles, etc.) and collisions due to environmental hazards usually resulting in the bicycle rider's fall. The MARG sensor used in our proposed system consists of a tri-axial magnetometer, a tri-axial accelerometer, and a tri-axial gyroscope sensor. The MARG sensor can also provide the orientation information (yaw, pitch, and roll angles) [30]–[33] and it does not require additional signal processing techniques such as Kalman-based algorithms [32], [34], [35]. The orientation measurements from the MARG sensor can enhance the accuracy of a fall detection system compared to the methods which only use the acceleration data [32]. Specifically, to detect bicycle accidents, our proposed method first obtains features based on average and standard deviation values from acceleration signals, angular velocity signals, angle signals, and magnitude signals in X-, Y-, and Z- directions, respectively. The proposed system applies principal component analysis (PCA), which has been widely used in engineering fields to reduce the dimensionality [16], [20]–[22], [36], [37], to these 24 MARG features to reduce their dimensionality. To classify bicycle accident events, the proposed system adopts support vector machines (SVM), which has been widely used for classification in science and engineering studies [16], [21], [27], [38]–[41]. The rest of this article is organized as follows: Section II describes the materials for our proposed accident detection system. Section III explains our proposed accident detection system. Our experimental results are described in Section IV, and finally, Section V concludes this article.

II. Materials

A. Hardware Setup

We designed the hardware module and attached it to the handlebar of a bicycle as shown in Fig. 1 to acquire raw MARG signals. The designed hardware can find the orientation of the bicycle using the MARG data. The proposed hardware consists of five components: 1) microcontroller, 2) sensing, 3) storage, 4) transmission, and 5) power supply units (see details in Subsection III-A). These five components are assembled in a single module and covered by a 3D printed case using the MakerBot Method 3D printer [42] with acrylonitrile butadiene styrene (ABS) material [43]. Especially, this case is designed to provide protection from physical damages and water. Our detailed hardware design is described in Subsection III-A.

B. Experimental Protocol

The data related to riding status which can be cycling or falling status in this article was acquired from the MARG sensor mounted on the bicycle shown in Fig. 1. We followed the Texas Tech University Institutional Review Board (IRB) (IRB#: IRB2019-1248) for this data acquisition. Cycling status and falling status were emulated on three different types of terrains shown in Fig. 2: 1) grassy terrain (straight), 2) cement terrain (straight, uphill, and downhill), and 3) gravel terrain (uphill, and downhill). We started from emulating cycling status with an average speed of 6 miles per hour (mph) and then emulated falling status by leaving the bicycle to fall. The net force on the bicycle was applied in two different ways: 1) pushing the bicycle while holding the handle to increase the speed of the bicycle from 6 mph to 9 mph, and 2) by squeezing a brake lever to decrease the speed from 6 mph to 0 mph. There was no rider on the bicycle when the fall status (or fall accident) was emulated. The fall accidents were emulated in left (L), right (R), forward (F), or backward (B) directions. In total, we conducted 34 combinations of trials shown in Fig. 2. Specifically, we emulated six trials for each of the grassy and cement terrains in a straight direction. For the uphill and downhill directions of the cement terrain, we conducted five and six trials, respectively. In addition, five trials were emulated for the uphill gravel terrain, and six trials for the downhill gravel terrain. Each trial included one phase of cycling status and one phase of falling status. The duration of each status was not fixed but different in each trial. The entire duration of 34 trials was 31 minutes and the summation of the duration of falling status among 31 minutes was 11 minutes. All the trials were conducted using a single bicycle.

C. Pre-Calibration and Preprocessing

Since accelerometer and magnetometer sensors can have bias errors which can lead to inaccurate data measurement, we pre-calibrated these sensors by using the software provided by the manufacturer (Shenzhen Wit Intelligent [44]) after connecting the sensors to a computer. For example, we pre-calibrated the accelerometer sensor by setting the accelerometer value to 0 when the sensor was in a fixed location. The accelerometer, magnetometer, and gyroscope sensors are sensitive to unwanted noise which may lead to unreliable feature extraction. Hence, we filtered the unwanted noise signal with a moving average filter operation, i.e., $y_F(i) = \frac{1}{2N+1}(y(i+N) + y(i+N-1) + y(i-N))$ where $y(i)$ is a data point of the raw signal, $y_F(i)$ is the filtered data point of $y(i)$, N is the number of neighboring data points on either side, and $2N+1$ is the window size. In this article, we set N to be 1 to make the window size $2N+1$ to be 3.

III. Proposed Accident Detection System

The hardware and software of our proposed accident detection system for bicycle riders are described in detail in Subsections III-A, and III-B, respectively.

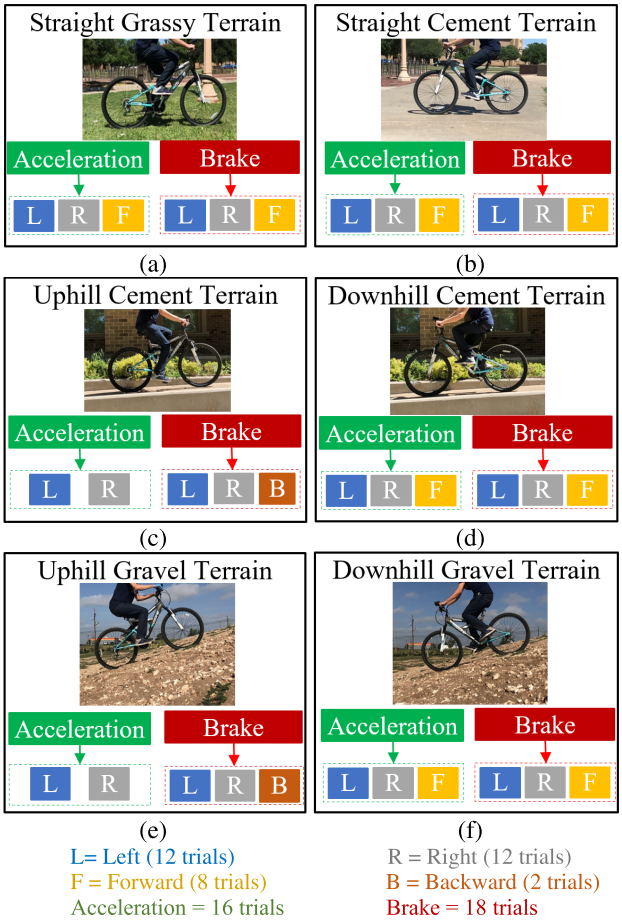

Fig. 2. Combination of different terrains, directions, and motion conditions where the fall accidents occurred in our experiments.

A. Design of Hardware Module

The hardware module of the proposed system (see Fig. 3) has five units as follows:

1) Microcontroller Unit: The microcontroller unit is a central hardware unit in our proposed system. Arduino Nano [45] shown in Fig. 3 is used as the microcontroller unit of our system. Arduino Nano is based on the ATmega328P. Arduino Nano is an Advanced Virtual RISC (AVR) microcontroller and it is light, small, robust, and consumes low power. Our microcontroller unit converts analog signals captured by a sensing unit to digital data using its analog to digital converter (ADC) and transfers the digital data to the storage unit. Specifically, the ADC in the microcontroller unit maps analog voltage values (0 - 5 V) to digital values (0 to 1023) [46]. The maximum sampling rate of the Arduino Nano's ADC clock is 125 kHz.

2) Sensing Unit: The sensor unit measures different types of information: acceleration, angular velocity, angle, and magnitude signals. The WT901 sensor module [47] is used as the sensor unit of our system which has tri-axial accelerometer, gyroscope, and magnetometer sensors. The WT901 sensor manufactured by Shenzhen Wit Intelligent [44] is equipped with a built-in microprocessor that also has an embedded Kalman filter algorithm. The WT901's clock line (SCL) pin and its data line (SDA) pin were connected to the Arduino Nano's analog pins (A4 and A3), respectively. The voltage

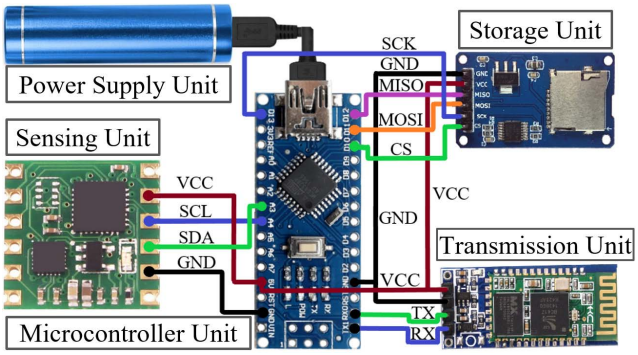

Fig. 3. Schematic of connections between the five units of the hardware module.

common collector (VCC) pin of the WT901 was connected to the 5V pin of the Arduino Nano and their ground (GND) pins together.

3) Storage Unit: Since the sensor unit does not have storage, we added the storage unit which used a 64 GB Micro SD storage memory board manufactured by Adafruit Industries (NY, USA) [48]. The VCC pin of the memory board was connected to the Arduino Nano's 5V pin and their GND pins were connected to each other. The chip select (CS), master out slave in (MOSI), master in slave out (MISO), and serial clock (SCK) pins of the storage unit were connected to the I/O pins (D10, D11, D12, and D13) of the Arduino Nano, respectively.

4) Transmission Unit: The transmission unit sends the data wirelessly to the computer (Acer Veriton M4640G [49]) for further signal processing. Specifically, the DSD Tech HM-10 Bluetooth 4.0 module (DSD TECH Team, China [50]) is used as the transmission unit of our system. The DSD Tech HM-10 has a Bluetooth 4.0 module with four pins. The serial data input (RX) pin of the Bluetooth module was connected to the serial data output (TX) pin of Arduino Nano. The TX pin of the Bluetooth module was connected to the RX pin of the Arduino Nano. The VCC pin of the Bluetooth module was connected to the 5V pin of the Arduino Nano and the GND pins together.

5) Power Supply Unit: The power supply unit in our proposed system is a 5 V, 2200 milliampere-hour (mAh) Lithium-Ion Battery (HY-10995-BLK, HYPE^{TM}, China), and it is directly connected to Arduino Nano through the Universal Serial Bus (USB) port. The sensing, storage, and transmission units were connected through the VCC and GND pins to Arduino Nano to get the power. Considering the power consumption of all the units (450 milliwatt-hours (mWh)) [45], [47], [48], [50] and the stored energy of the power supply (11000 mWh), the system operates for around 24 hours (11000/450 $\cong$ 24.4) before it is completely discharged.

B. Design of Software

1) Feature Extraction: The software module in our proposed system first segments the obtained signals into segments with the length of L_S, and then calculates features from each segment. Here, the value L_S is set by the grid search algorithm [51], [52] in a suboptimal way, i.e., the L_S value giving the highest performance from $L_S = 1$ to $L_S = 7$ with

the step size of 1 second is chosen. It is shown that the average (AVG) and the standard deviation (SD) values of the signals are effective in discriminating the fall status [16]. Hence, we derived AVG_{Acc} and SD_{Acc} from the acceleration signals, AVG_{AV} and SD_{AV} from the angular velocity signals, AVG_{Ang} and SD_{Ang} from the angle signals, and AVG_{Mag} and SD_{Mag} from the magnitude signals for X-, Y-, and Z- directions which become 24 features in total. Denoting a feature matrix by $\boldsymbol{X}_{m\times n}$ where m is the number of segments and n is the number of features, $\boldsymbol{X}_{m\times n}$ was divided into training and validation set ($\boldsymbol{R}_{p\times n}$, $p = 80\%$ of m) and testing set ($\boldsymbol{S}_{q\times n}, q = 20\%$ of m). In this article, we used 5-fold cross-validation to find the optimum parameters of the SVM model.

2) Feature Reduction: We used PCA to reduce the computational complexity by decreasing the dimensionality of the features. For our detection algorithm, the computational time required for detecting bicycle fall accidents is reduced by this PCA while the detection accuracy is maintained. To perform PCA and avoid data leakage in the model, the PCA components need to be calculated for the training and test datasets, separately [53], [54]. The training matrix ($\boldsymbol{T}_{k\times n}$) for each fold was derived from the matrix of training and validation set ($\boldsymbol{R}_{p\times n}$) where k is equal to 80% of p. We first made $\boldsymbol{T}_{k\times n}$ centered to form an unbiased matrix $\boldsymbol{A}_{k\times n}$ by subtracting the average of the j^{th} column ($\overline{\mu}_j$) from each column of the training matrix $\boldsymbol{T}$. Denoting by $\boldsymbol{C}$ the covariance matrix of $\boldsymbol{A}_{k\times n}$, we calculated the eigenvectors ($\boldsymbol{v}_j$) and its corresponding eigenvalues ($\boldsymbol{\lambda}_j$) of $\boldsymbol{S}$ and ordered them in a decreasing form ($\boldsymbol{\lambda}_1 \geq \boldsymbol{\lambda}_2 \geq \ldots \geq \boldsymbol{\lambda}_m$). The matrix of the major components $\boldsymbol{P}_{k\times l}$ was derived from the projection of the matrix $\boldsymbol{A}$ on the selected eigenvectors, where k is the number of training samples and l is the number of selected components. The number of selected components (l) was found by choosing the eigenvectors having larger eigenvalues. For this purpose, we set the PCA to keep only the components that explain 95% of the variance ($\boldsymbol{\lambda}_1 + \boldsymbol{\lambda}_2 + \ldots + \boldsymbol{\lambda}_l = 95\%$). We found 95% of the variance as an optimum value since the higher values ($\boldsymbol{\lambda}_1 + \boldsymbol{\lambda}_2 + \ldots + \boldsymbol{\lambda}_l > 95\%$) could result in overfitting. On the other hand, we may remove useful dimensions by choosing the lower values ($\boldsymbol{\lambda}_1 + \boldsymbol{\lambda}_2 + \ldots + \boldsymbol{\lambda}_l < 95\%$).

3) Classification: SVM has been widely applied in fall detection studies [16], [21], [27], [38]–[41]. We used SVM to classify the PCA values ($\boldsymbol{P}_{k\times l}$) obtained in Subsection III-B-2 into cycling status ($\boldsymbol{y}_i = 1$) and falling status ($\boldsymbol{y}_i = -1$). Denoting by $\boldsymbol{p}_i$ the i^{th} row of the training dataset ($\boldsymbol{P}_{k\times l}$) as the input vector, we aimed to find the optimal SVM model. Since the input vectors were not linearly separable, we used the Gaussian kernel function as an optimum solution among the nonlinear SVM kernels such as polynomial SVM kernels. The Gaussian kernel function ($K\left(\boldsymbol{p}_i, \boldsymbol{p}\right)$) is defined as follows:

$$K\left(p_i, p\right) = \exp\left(\frac{-\left\|\boldsymbol{p} - \boldsymbol{p}_i\right\|^2}{2\sigma^2}\right), \tag{1}$$

where σ is the kernel scale. We found $\sigma = 1.2$ (search range: 0.1-1.5) as the optimal value using 5-fold cross-validation.

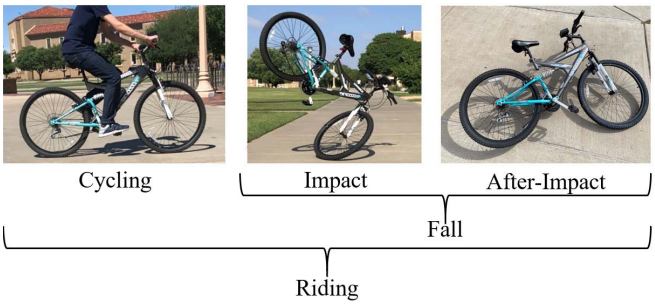

Fig. 4. An example of the cycling status and fall status. The falling status consists of the impact moment and after-impact duration.

After the decision boundary of the SVM model was acquired and validated, it was used to classify the PCA components of the unknown test vector ($\boldsymbol{S}_{q\times n}$) to cycling or fall status. The PCA component matrix of test data ($\boldsymbol{U}_{q\times l}$) where q is the number of testing samples and l is the number of selected components was calculated using the same procedure explained in Subsection III-B-2.

IV. Results

We applied our proposed algorithm to 34 riding trials, each of which consisted of cycling status and fall status. The fall status was divided into two phases [32]: 1) the *impact phase* indicating the moment when the fall occurs, and 2) the *after-impact phase* indicating the period during which the bicycle falls down and is no longer in motion after the fall occurs. Fig. 4 shows an example of each phase of a riding trial.

A. Effects of Fall Accident on Signals

Figs. 5-8 show examples of raw acceleration, angular velocity, angle, and magnitude signals (upper) and SD and AVG (lower) of the signals which were calculated based on segment-by-segment calculations, where the length of each segment is 2 seconds ($L_S = 2$). Here, the bicycle was run on straight grassy terrain with a cycling status from $t = 0$ to $t = 22$ and a falling status from $t = 22$ to $t = 35$.

Fig. 5a, Fig. 5b, and Fig. 5c show the acceleration signals, and their corresponding SD_{Acc}, AVG_{Acc} features, respectively. Fig. 5b shows that $SD_{\text{Acc,Y}}$ has higher values compared to $SD_{\text{Acc,X}}$ and $SD_{\text{Acc,Z}}$ when there is an impact at $t = 22$. Moreover, as shown in Fig. 5c, there is a larger variation in $AVG_{\text{Acc,Y}}$ compared to $AVG_{\text{Acc,X}}$ and $AVG_{\text{Acc,Z}}$ values when there is an impact at $t = 22$. Hence, Fig. 5 shows that the fall that occurred in the Y- direction is reflected in the $SD_{\text{Acc,Y}}$ and $AVG_{\text{Acc,Y}}$ values.

Fig. 6 shows an example of the angular velocity signals with their corresponding SD_{AV} and AVG_{AV} features. As shown in Fig. 6a, the angular velocity signal has more variations in the Z- direction compared to the X- and Y- directions during the impact phase ($t = 22$s to $t = 25$). These variations in the Z- direction reflect the rotation of the bicycle handlebar. This rotation is also reflected by the angle signal shown in Fig. 7a, which shows sharp changes in the Z-direction during the impact phase ($t = 22$ to $t = 25$). As a result, $SD_{\text{Ang,Z}}$ has higher variations compared to $SD_{\text{Ang,X}}$, $SD_{\text{Ang,Y}}$ values, as shown in Fig. 7b.

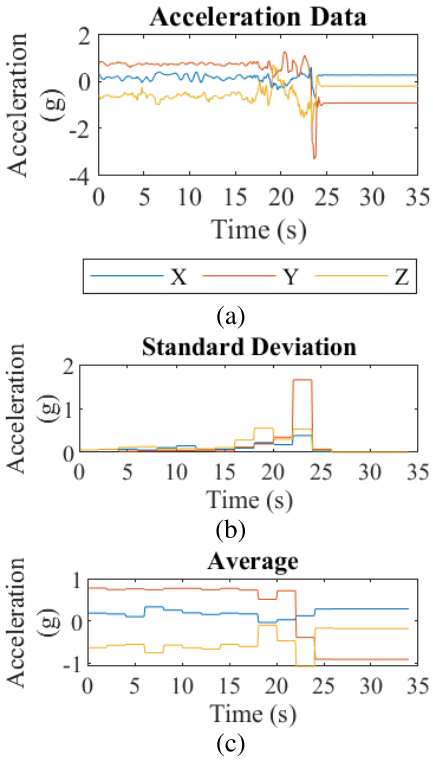

Fig. 5. An example of accelerometer signals with associated standard deviation and average features. Here, cycling phase is from $t = 0$ to $t = 22$ while fall phase starts at $t = 22$ to $t = 35$. (a) Extracted signals, (b) standard deviation features, and (c) average features.

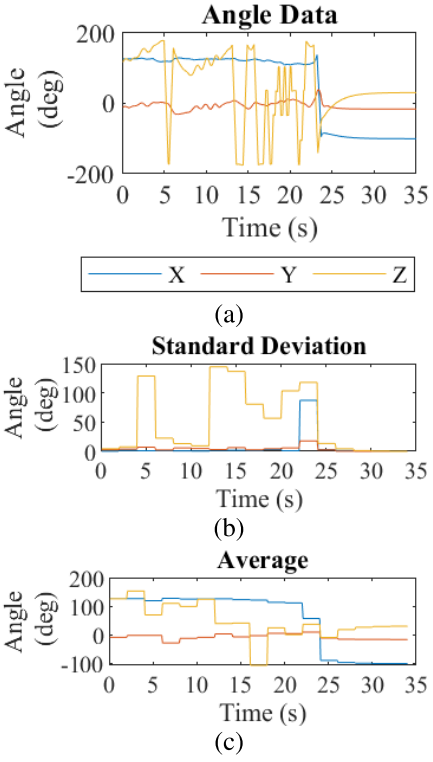

Fig. 7. An example of angle signals with the associated standard deviation and average features. Here, the cycling phase is from $t = 0$ to $t = 22$ while the fall phase starts at $t = 22$ to $t = 35$. (a) Extracted signals, (b) standard deviation features, and (c) average features.

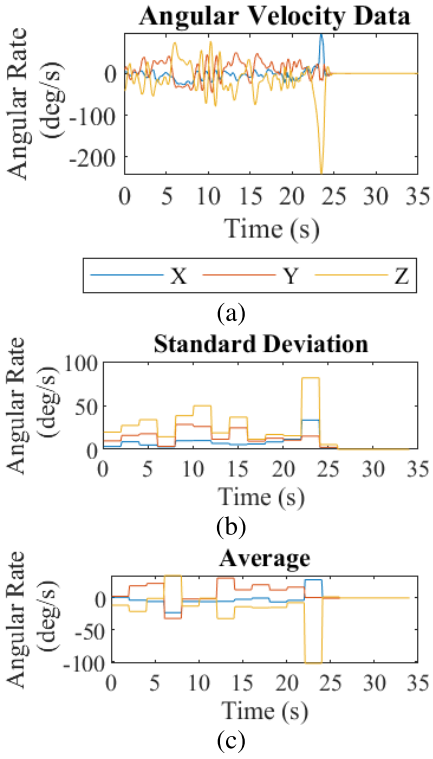

Fig. 6. An example of angular velocity signals with the associated standard deviation and average features. Here, cycling phase is from $t = 0$ to $t = 22$ while fall phase starts at t = 22 to $t = 35$. (a) Extracted signals, (b) standard deviation features, and (c) average features.

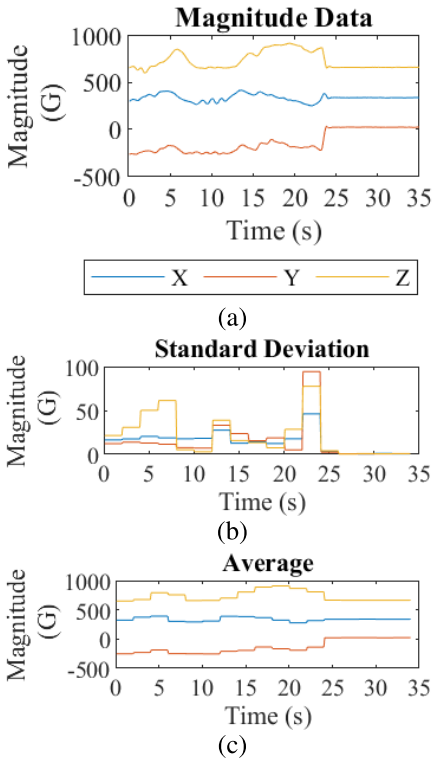

Fig. 8. An example of magnitude signals with the associated standard deviation and average features. Here, the cycling phase is from $t = 0$ to $t = 22$ while the fall phase starts at $t = 22$ to $t = 35$. (a) Extracted signals, (b) standard deviation features, and (c) average features.

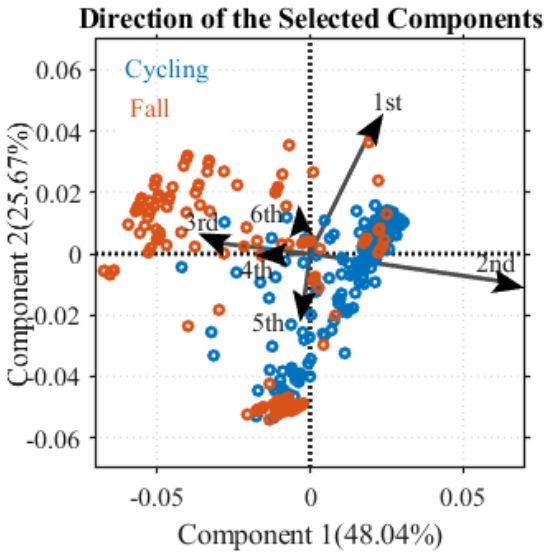

Fig. 9. Representation of data with the first six extracted features.

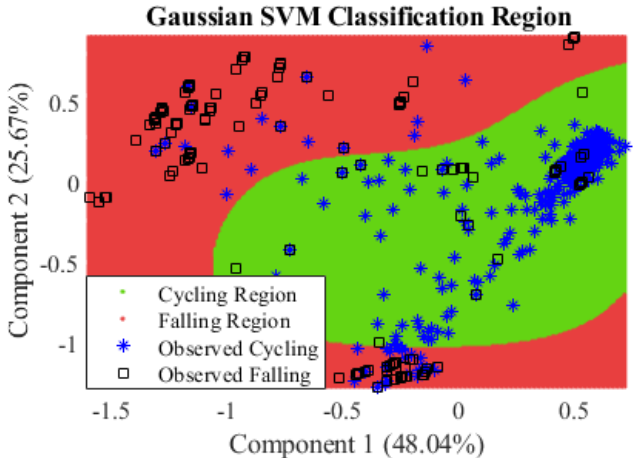

Fig. 10. The SVM decision region classifying the data into cycling and falling regions. The green region is the SVM classification region for cycling data, while the red region is the SVM classification region for falling data.

Fig. 8 shows the magnitude signals and their corresponding SD_{Mag} and AVG_{Mag} features. It is shown in Fig. 8b that the simulated fall has affected the Y- direction value $SD_{Mag,Y}$ more compared to the values in the X- and Z- directions, which reflects that the fall occurred in Y- direction.

B. PCA-Based Feature Reduction

Figs. 5-8 show that some of the 24 features play important roles in discriminating fall events while the other features do not. In this article, to reduce computational complexity, we chose the most crucial 6 features (or components) out of the 24 features using PCA explained in Section III-B. Before performing this PCA, we normalized all the features to have values between +1 and -1. The PCA in our proposed algorithm chose 6 components among the 24 components, as shown in Fig. 9, which explain 48.04%, 25.67%, 10.25%, 7.19%, 3.72%, and 1.60%, respectively.

TABLE I
CONFUSION MATRIX OF OUR PROPOSED CLASSIFICATION ALGORITHM

	Cycling	Fall
Cycling	268	12
Fall	6	94

C. SVM-Based Fall Detection

The SVM in our proposed algorithm, which is explained in Section III-B, is applied to 380 input unknown data segments consisting of cycling and fall statuses. As a result, Fig. 10 shows the SVM decision boundary with the feature data, which considers cycling and falling status data. Table I demonstrates that cycling and falling statuses are classified accurately with 95.2% accuracy, 96% sensitivity, and 94% specificity.

V. DISCUSSION AND CONCLUSION

In this article, we have proposed a bicycle accident detection system consisting of hardware and software modules. For this purpose, we conducted 34 riding trials, each of which includes cycling status and fall status segments. To detect fall events from cycling events, we considered time-domain features, i.e., AVG and SD of accelerometer, angular velocity, angle, and magnitude signals in X-, Y-, and Z-directions, which resulted in 24 features. To decrease the dimensionality of data, we have applied PCA to these 24 features. As a result, 6 components have been chosen to be used as input of our SVM classifier.

Compared to previous studies [9]–[11], we have focused on detecting fall accidents for the bicycle riders. Table II shows the comparison of our proposed algorithm to the previous studies in [9]–[11] in terms of cycling devices, accidents, classifiers, and sensors. In [9], [10], the accident prevention-related algorithms [48] were proposed for bicycles. However, they do not detect fall accidents, rather they recognize cycling behavior only. Meanwhile, in [11], a fall accident detection system was proposed not for bicycles but motorcycles. The classification algorithms adopted in [9] and [10] were ensemble learning and transfer kernel learning classifiers, respectively [48]. On the other hand, in [11], the accident detection system was based on the threshold algorithms. Our proposed system detects fall accidents using the SVM classifier and achieved 95.2% accuracy, which is higher compared to those of [9]–[11]. From the viewpoint of sensors, [9]–[11] adopted accelerometer and gyroscope sensors to acquire data while we used the MARG sensor which provides more accurate information regarding cycling and falling compared to using accelerometer and gyroscope sensors only. Finally, [9], [10] assumed that riders use smartphones to acquire the data and the detection systems were tied to those devices. In this article, we designed a hardware module that is mounted on the bicycle handlebar which provides a comprehensive fall detection system giving users the freedom to keep their smartphones in a pocket, bag, or any other preferred places while cycling. Our proposed hardware module is protected from hard impacts, rain, and water with a designed 3D case. This was another improvement

TABLE II
COMPARISON OF THE PROPOSED FALL DETECTION SYSTEM WITH CONVENTIONAL SYSTEMS

Study	Cycling device	Detected accidents	Classifier	Sensors
Our system	Bicycle	Fall	SVM	MARG sensor
[10]	Bicycle	Lane weaving, standing pedaling	Transfer kernel learning	Accelerometer, gyroscope
[9]	Bicycle	Stop, run straight, turn right, turn left	Ensemble learning	Accelerometer, gyroscope
[11]	Motorcycles	Near fall scenarios, naturalistic riding scenarios	Threshold-based algorithm	Accelerometer, gyroscope

included in our detection system as not all smartphones may be protected from crash impacts. Simply designing a 3D protective case for smartphones may not be a feasible solution since there would be a need to design a specific case for each model of phone available on the market.

Our designed hardware module was equipped with a power supply that provides its power to the system for more than 24 hours continuously (or 12 days considering for 2 hours/day cycling activity) before being discharged. Moreover, users can easily transfer stored data using the Bluetooth unit to the processing station (computer/laptop) without removing the module from the handlebar and assembling it again for each data transmission process.

In future, we plan to use physiological signals such as photoplethysmogram (PPG), electrocardiogram (ECG), and peripheral oxygen saturation (SpO2) in detecting the severity of the accident. Moreover, the GPS data will be used to locate the position of the accident. These signals also provide information that can be used to predict the fall accident based on cycling behavior. Moreover, the Bluetooth module can be used to transfer the information to smartphone or smartwatch applications or send an alert through the smartphone to an emergency center.

REFERENCES

[1] *Centers for Disease Control and Prevention (CDC)*. Bicycle Safety. Accessed: 2019. [Online]. Available: https://www.cdc.gov/motorvehiclesafety/bicycle/index.html

[2] M. J. Thompson and F. P. Rivara, "Bicycle-related injuries," *Amer. Family Physician*, vol. 63, no. 10, pp. 2007–2013, 2001.

[3] J. Rogé, D. Ndiaye, I. Aillerie, S. Aillerie, J. Navarro, and F. Vienne, "Mechanisms underlying cognitive conspicuity in the detection of cyclists by car drivers," *Accident Anal. Prevention*, vol. 104, pp. 88–95, Jul. 2017, doi: 10.1016/j.aap.2017.04.006.

[4] A. Fanca, A. Puscasiu, S. Folea, and H. Valean, "Trauma accident detecting and reporting system," in *Proc. IEEE Int. Conf. Autom., Qual. Test., Robot. (AQTR)*, May 2018, pp. 1–5.

[5] S. Smaldone, C. Tonde, V. Ananthanarayanan, A. Elgammal, and L. Iftode, "Improving bicycle safety through automated real-time vehicle detection," RUcore: Rutgers Univ. Community Repository, New Brunswick, NJ, USA, Tech. Rep. DCS-TR-665, 2010, doi: 10.7282/T3FX7DX5.

[6] S. Kawanaka, Y. Kashimoto, A. Firouzian, Y. Arakawa, P. Pulli, and K. Yasumoto, "Approaching vehicle detection method with acoustic analysis using smartphone for elderly bicycle driver," in *Proc. 10th Int. Conf. Mobile Comput. Ubiquitous Netw. (ICMU)*, Oct. 2017, pp. 1–6.

[7] J. J. Anaya, E. Talavera, D. Gimenez, N. Gomez, F. Jimenez, and J. E. Naranjo, "Vulnerable road users detection using V2X communications," in *Proc. IEEE 18th Int. Conf. Intell. Transp. Syst.*, Sep. 2015, pp. 107–112, doi: 10.1109/ITSC.2015.26.

[8] K. Fukushima and K. Matsushima, "Robust multi-directional bicycle recognition on the rotation using the stereo vision," in *Proc. IEEE Int. Conf. Veh. Electron. Saf. (ICVES)*, Nov. 2015, pp. 36–40, doi: 10.1109/ICVES.2015.7396890.

[9] Y. Usami, K. Ishikawa, T. Takayama, M. Yanagisawa, and N. Togawa, "Bicycle behavior recognition using sensors equipped with smartphone," in *Proc. IEEE 8th Int. Conf. Consum. Electron. Berlin (ICCE-Berlin)*, Sep. 2018, pp. 1–6, doi: 10.1109/ICCE-Berlin.2018.8576254.

[10] W. Gu *et al.*, "BikeMate: Bike riding behavior monitoring with smartphones," in *Proc. 14th EAI Int. Conf. Mobile Ubiquitous Systems: Comput., Netw. Services*, Nov. 2017, pp. 313–322, doi: 10.1145/3144457.3144462.

[11] D. Selmanaj, M. Corno, and S. M. Savaresi, "Hazard detection for motorcycles via accelerometers: A self-organizing map approach," *IEEE Trans. Cybern.*, vol. 47, no. 11, pp. 3609–3620, Nov. 2017, doi: 10.1109/TCYB.2016.2573321.

[12] N. Watthanawisuth, T. Lomas, and A. Tuantranont, "Wireless black box using MEMS accelerometer and GPS tracking for accidental monitoring of vehicles," in *Proc. IEEE-EMBS Int. Conf. Biomed. Health Informat.*, Jan. 2012, pp. 847–850.

[13] F. Attal, A. Boubezoul, L. Oukhellou, N. Cheifetz, and S. Espie, "The powered two wheelers fall detection using multivariate CUmulative SUM (MCUSUM) control charts," in *Proc. 17th Int. IEEE Conf. Intell. Transp. Syst. (ITSC)*, Oct. 2014, pp. 1280–1285.

[14] S. V. Georgakopoulos, S. K. Tasoulis, I. Maglogiannis, and V. P. Plagianakos, "On-line fall detection via mobile accelerometer data," in *Proc. IFIP Int. Conf., Artif. Intell. Appl. Innov.* Bayonne, France: Springer, 2015, pp. 103–112.

[15] B. Aguiar, T. Rocha, J. Silva, and I. Sousa, "Accelerometer-based fall detection for smartphones," in *Proc. IEEE Int. Symp. Med. Meas. Appl. (MeMeA)*, Jun. 2014, pp. 1–6.

[16] A. Jahanjoo, M. N. Tahan, and M. J. Rashti, "Accurate fall detection using 3-axis accelerometer sensor and MLF algorithm," in *Proc. 3rd Int. Conf. Pattern Recognit. Image Anal. (IPRIA)*, Apr. 2017, pp. 90–95.

[17] M. Mubashir, L. Shao, and L. Seed, "A survey on fall detection: Principles and approaches," *Neurocomputing*, vol. 100, pp. 144–152, Jan. 2013.

[18] O. Aziz, M. Musngi, E. J. Park, G. Mori, and S. N. Robinovitch, "A comparison of accuracy of fall detection algorithms (threshold-based vs. Machine learning) using waist-mounted tri-axial accelerometer signals from a comprehensive set of falls and non-fall trials," *Med. Biol. Eng. Comput.*, vol. 55, no. 1, pp. 45–55, Jan. 2017.

[19] F. Bagalà *et al.*, "Evaluation of accelerometer-based fall detection algorithms on real-world falls," *PLoS ONE*, vol. 7, no. 5, May 2012, Art. no. e37062.

[20] C. Park, J. Kim, and H.-J. Choi, "A watch-type human activity detector for the aged care," in *Proc. 14th Int. Conf. Adv. Commun. Technol. (ICACT)*, Feb. 2012, pp. 648–652.

[21] G. Shi, Y. Zou, Y. Jin, and W. Jung Li, "PCA/ICA-based SVM for fall recognition using MEMS motion sensing data," in *Proc. APCCAS IEEE Asia Pacific Conf. Circuits Syst.*, Nov. 2008, pp. 69–72.

[22] N. T. Hai and T. H. An, "PCA-SVM algorithm for classification of skeletal data-based eigen postures," *Am. J. Biomed. Eng*, vol. 6, pp. 47–158, 2016.

[23] A. Akbar Safavi, A. Keshavarz-Haddad, S. Khoubani, S. Mosharraf-Dehkordi, A. Dehghani-Pilehvarani, and F. Sadat Tabei, "A remote elderly monitoring system with localizing based on wireless sensor network," in *Proc. Int. Conf. Comput. Design Appl.*, Jun. 2010, pp. V2-553–V2-557.

[24] M. Saleh and R. L. B. Jeannes, "Elderly fall detection using wearable sensors: A low cost highly accurate algorithm," *IEEE Sensors J.*, vol. 19, no. 8, pp. 3156–3164, Apr. 2019.

[25] S. Abbate, M. Avvenuti, F. Bonatesta, G. Cola, P. Corsini, and A. Vecchio, "A smartphone-based fall detection system," *Pervas. Mobile Comput.*, vol. 8, no. 6, pp. 883–899, Dec. 2012.

[26] F. J. S. Thilo, S. Hahn, R. J. G. Halfens, and J. M. G. A. Schols, "Usability of a wearable fall detection prototype from the perspective of older people—A real field testing approach," *J. Clin. Nursing*, vol. 28, nos. 1–2, pp. 310–320, Jan. 2019.

[27] L.-J. Kau and C.-S. Chen, "A smart phone-based pocket fall accident detection, positioning, and rescue system," *IEEE J. Biomed. Health Informat.*, vol. 19, no. 1, pp. 44–56, Jan. 2015, doi: 10.1109/JBHI.2014.2328593.

[28] J.-S. Lee and H.-H. Tseng, "Development of an enhanced threshold-based fall detection system using smartphones with built-in accelerometers," *IEEE Sensors J.*, vol. 19, no. 18, pp. 8293–8302, Sep. 2019, doi: 10.1109/JSEN.2019.2918690.
[29] M. V. Albert, K. Kording, M. Herrmann, and A. Jayaraman, "Fall classification by machine learning using mobile phones," *PLoS ONE*, vol. 7, no. 5, May 2012, Art. no. e36556, doi: 10.1371/journal.pone.0036556.
[30] S. O. H. Madgwick, A. J. L. Harrison, and R. Vaidyanathan, "Estimation of IMU and MARG orientation using a gradient descent algorithm," in *Proc. IEEE Int. Conf. Rehabil. Robot.*, Jun. 2011, pp. 1–7, doi: 10.1109/ICORR.2011.5975346.
[31] V. Cotechini, A. Belli, L. Palma, M. Morettini, L. Burattini, and P. Pierleoni, "A dataset for the development and optimization of fall detection algorithms based on wearable sensors," *Data Brief*, vol. 23, Apr. 2019, Art. no. 103839.
[32] P. Pierleoni, A. Belli, L. Palma, M. Pellegrini, L. Pernini, and S. Valenti, "A high reliability wearable device for elderly fall detection," *IEEE Sensors J.*, vol. 15, no. 8, pp. 4544–4553, Aug. 2015, doi: 10.1109/JSEN.2015.2423562.
[33] L. Wohle, S. Miller, J. Gerken, and M. Gebhard, "A robust interface for head motion based control of a robot arm using MARG and visual sensors," in *Proc. IEEE Int. Symp. Med. Meas. Appl. (MeMeA)*, Jun. 2018, pp. 1–6, doi: 10.1109/MeMeA.2018.8438699.
[34] D. M. Karantonis, M. R. Narayanan, M. Mathie, N. H. Lovell, and B. G. Celler, "Implementation of a real-time human movement classifier using a triaxial accelerometer for ambulatory monitoring," *IEEE Trans. Inf. Technol. Biomed.*, vol. 10, no. 1, pp. 156–167, Jan. 2006, doi: 10.1109/TITB.2005.856864.
[35] P. Pierleoni *et al.*, "A wearable fall detector for elderly people based on AHRS and barometric sensor," *IEEE Sensors J.*, vol. 16, no. 17, pp. 6733–6744, Sep. 2016, doi: 10.1109/JSEN.2016.2585667.
[36] R. M. Gibson, A. Amira, N. Ramzan, P. Casaseca-de-la-Higuera, and Z. Pervez, "Matching pursuit-based compressive sensing in a wearable biomedical accelerometer fall diagnosis device," *Biomed. Signal Process. control*, vol. 33, pp. 96–108, Mar. 2017.
[37] B. Ando, S. Baglio, C. O. Lombardo, and V. Marletta, "An event polarized paradigm for ADL detection in AAL context," *IEEE Trans. Instrum. Meas.*, vol. 64, no. 7, pp. 1814–1825, Jul. 2015, doi: 10.1109/TIM.2014.2385144.
[38] A. Y. Alaoui, S. El Fkihi, and R. O. H. Thami, "Fall detection for elderly people using the variation of key points of human skeleton," *IEEE Access*, vol. 7, pp. 154786–154795, 2019, doi: 10.1109/ACCESS.2019.2946522.
[39] S. S. Kambhampati, M. S. Manikandan, V. Singh, and B. Ramkumar, "Unified framework for triaxial accelerometer-based fall event detection and classification using cumulants and hierarchical decision tree classifier," *Healthcare Technol. Lett.*, vol. 2, no. 4, pp. 101–107, Aug. 2015, doi: 10.1049/htl.2015.0018.
[40] M. Huang, X. Wang, P. Sun, S. Wang, and Z. Wang, "Wavelet package analysis based fall detection and diagnosis," in *Proc. 37th Chin. Control Conf. (CCC)*, Jul. 2018, pp. 4206–4211, doi: 10.23919/ChiCC.2018.8483116.
[41] F. Hossain, M. L. Ali, M. Z. Islam, and H. Mustafa, "A direction-sensitive fall detection system using single 3D accelerometer and learning classifier," in *Proc. Int. Conf. Med. Eng., Health Informat. Technol. (MediTec)*, Dec. 2016, pp. 1–6, doi: 10.1109/MEDITEC.2016.7835372.
[42] *MakerBot METHOD Printer*. Accessed: Jan. 22, 2020. [Online]. Available: https://store.makerbot.com/3d-printers/printers/method/bundles/method/?utm_source=google&utm_medium=cpc&utm_campaign=gs_brand_printers_exact&gclid=CjwKCAiAgqDxBRBTEiwA59eENxbmifquP7rE_9iicSmoyuBRQiRfdEjfXbZAQJHf3najSp9Pglsf0hoC44wQAvD_BwE
[43] *Black MH Build Series ABS Filament*. Accessed: Jun. 30, 2020. [Online]. Available: https://www.matterhackers.com/store/3d-printer-filament/175mm-abs-filament-black-1-kg
[44] *Shenzhen Wit Intelligent Co., Ltd*. Accessed: Jun. 24, 2020. [Online]. Available: http://www.wit-motion.com/english.php?m=text&a=index&classify_id=46402
[45] *Arduino, Arduino Nano*. Accessed: Dec. 11, 2019. [Online]. Available: https://www.arduino.cc/en/Guide/ArduinoNano
[46] *Arduino Nano Tech Specs*. Accessed: Jun. 18, 2020. [Online]. Available: https://store.arduino.cc/usa/arduino-nano
[47] *Wit-Motion*. Accessed: Dec. 11, 2019. [Online]. Available: http://www.wit-motion.com/english.php
[48] *Microsd Card Breakout Board+*. Accessed: Jun. 18, 2020. [Online]. Available: https://www.adafruit.com/product/254
[49] *Acer Veriton M4640G*. Accessed: Jun. 24, 2020. [Online]. Available: https://www.intel.com/content/www/us/en/products/devices-systems/desktops/pcs/acer-veriton-m4640g-i7670z-H32296242.html
[50] (2017). *DSD TECH HM-10 Bluetooth 4.0*. [Online]. Available: http://www.dsdtech-global.com/2017/08/hm-10.html
[51] C. Gold and P. Sollich, "Model selection for support vector machine classification," *Neurocomputing*, vol. 55, nos. l–2, pp. 221–249, 2003, doi: 10.1016/S0925-2312(03)00375-8.
[52] S. Han, C. Qubo, and H. Meng, "Parameter selection in SVM with RBF kernel function," in *Proc. World Automat. Congr.*, Puerto Vallarta, Mexico, 2012, pp. 1–4.
[53] T. Howley, M. G. Madden, M.-L. O'Connell, and A. G. Ryder, "The effect of principal component analysis on machine learning accuracy with high dimensional spectral data," in *Proc. Int. Conf. Innov. Techn. Appl. Artif. Intell.* Cambridge, U.K.: Springer, 2005, pp. 209–222.
[54] F. Wu, S. Yin, and H. R. Karimi, "Fault detection and diagnosis in process data using support vector machines," *J. Appl. Math.*, vol. 2014, pp. 1–9, 2014, doi: 10.1155/2014/732104.

Fatemehsadat Tabei (Graduate Student Member, IEEE) received the B.S. and M.S. degrees in electrical engineering from Shiraz University, Shiraz, Iran. She is currently pursuing the Ph.D. degree with Texas Tech University, USA. Her current research interests include biomedical signal processing, biomedical image processing, and machine learning.

Behnam Askarian (Graduate Student Member, IEEE) received the B.S. and M.S. degrees in electrical engineering from Shiraz University, Shiraz, Iran. He is currently pursuing the Ph.D. degree with Texas Tech University, USA. His current research interests include biomedical image processing, machine learning, and monitoring of health and disease using smartphones.

Jo Woon Chong (Member, IEEE) received the B.S., M.S., and Ph.D. degrees in electrical engineering from the Korea Advanced Institute of Science and Technology, Daejeon, South Korea. He was a Postdoctoral Fellow with the Massachusetts Institute of Technology (MIT) and a Research Assistant Professor with the Worcester Polytechnic Institute, USA. Since 2016, he has been an Assistant Professor with Texas Tech University, USA. His current research interests include biomedical signal processing, non-invasive physiological monitoring, sensors and wireless communication for medical care, machine learning techniques for healthcare data, and home monitoring of health and disease.